J. Electrochem. Sci. Eng. **14(3)** (2024) 353-368; http://dx.doi.org/10.5599/jese.2330

Open Access : : ISSN 1847-9286
https://pub.iapchem.org/ojs/index.php/JESE

Original scientific paper

Supercapacitive performance of self-assembled thin film of liquid catocene/basal plane pyrolytic graphite electrode

Sajjad Damiri✉, Zahra Samiei and Hamid R. Pouretedal

Department of Applied Chemistry, Malek-Ashtar University of Technology, Shahin-shahr, Esfahan, I.R. Iran

Corresponding author: ✉sajjaddamiri@chmail.ir; Tel: +98-314-591-2253; Fax: +98-314-522-0420

Received: March 21, 2024; Accepted: July 4, 2024; Published: July 23, 2024

Abstract

Reasonable design of electrode material with low cost, lightweight, and excellent electrochemical properties is of great significance for future large-scale energy storage applications. Herein, we report the electrochemical and supercapacitive behaviour of the liquid redox of catocene, 2,2'-bis(ethyl-ferroceneyl) propane, self-assembled on a basal plane pyrolitic graphite electrode in comparison to the solid ferrocene thin film in aqueous sodium sulfate electrolyte. The modified electrode surfaces were evaluated to assess the iron content and the formation of thin film using scanning electron microscopy, laser-induced breakdown spectroscopy, and attenuated total reflectance method. Also, the supercapacitive performances of the related modified electrodes were assessed and compared using cyclic voltammetry and galvanostatic charge-discharge in a three-electrode system and an asymmetric two-electrode supercapacitor system. Electrochemical results showed that the electrode processes are diffusion-controlled with battery-like behaviour, and the liquid catocene exhibits more effective interaction with the graphite surface in comparison to solid ferrocene. The catocene surface coverage on graphite is nearly 50-75 % higher than ferrocene, leading to improved interaction and charge transfer resistance, observed in electrochemical impedance spectroscopy studies. In galvanostatic charge-discharge evaluations, the supercapacitor based on catocene modified electrode shows a specific capacitance of 141.2 F g^{-1} at a current density of 1.0 A g^{-1}, with a specific energy density of 56.7 Wh kg^{-1} at a power density of 2.9 kW kg^{-1}.

Keywords

Supercapacitor; ferrocene; liquid redox; thin films; self-assembly

Introduction

Nowadays, with the development of new technologies and environmental concerns, there is an ever-increasing demand for clean, lightweight, high-capacity and cyclically stable electrical energy storage resources. In this regard, research and development on electrochemical supercapacitors (SCs)

have garnered special attention due to their high power density and long cycle life (>100,000 cycles), as well as rapid charge-discharge rates compared to batteries and fuel cells [1-3]. Electrochemical supercapacitors are classified into two main categories based on their energy storage mechanisms: 1) electrochemical double-layer capacitors, with the electric charge accumulating at the electrode/electrolyte interface, and 2) pseudo-capacitors, where charge is stored on electrochemically active sites through reversible redox reactions [4]. The research in designing new electrode materials is crucial to SCs because they play a pivotal role in the capacitive performance of SCs [5-7]. In the recent decade, various electrode active materials such as conducting polymers, transition metal oxides [4], metal complexes and metal-organic frameworks (MOFs) [8] have garnered attention due to their electrochemical behaviour and relatively desirable charge storage capacity. Furthermore, to lighten the weight and improve the surface area and electrical conductivity of the electrodes, various carbonaceous materials such as graphite, graphene, carbon nanotubes, carbon nanofibers [9], or porous metallic microstructures [10] have been developed.

Thin-film electrodes (TFEs), with relatively high charge-discharge rates and low equivalent series resistances (ESR), are a category of intelligent supercapacitor electrodes mainly used in portable and/or miniaturized devices [11]. However, the overall specific capacitance decreases due to the low loading of active material on these electrode surfaces. In this context, transition metal oxide (TMOs) thin films are usually high-capacity materials with high redox activity. However, their cyclability and poor rate performance are persistent challenges because of their dissolution in aqueous electrolytes and mediocre conductivity. A thin layer of RuO_2 as a noble metal oxide, with a thickness of 400 nm, shows a capacity of 4.5 F cm^{-2} at 2.0 mV s^{-1}, and it maintains nearly 90 % of the initial charge capacity after 10,000 charge-discharge cycles in micro-supercapacitors [12].

Nowadays, 2D metallic materials, including transition metal dichalcogenides (TMDs) [13] and MXene, with the general formula M_n+1X_n (M is an early transition metal, and X is C or N) [14], have been introduced as excellent options in TFEs. The TaS_2-based TMD electrode exhibits a high volumetric capacity close to 508 F cm^{-3} at a scan rate of 10 mV s^{-1} and its energy density in micro-supercapacitors is 58.5 Wh L^{-1} [15]. Ti_3C_2Tx MXene film with a Fe_3O_4 porous layer on a flexible Ni strip demonstrates electrochemical performance of 46.4 mF cm^{-2} at a current density of 0.5 mA cm^{-2}, and energy density of 0.970 μWh cm^{-2} at a power density of 0.176 mW cm^{-2}, with good cycle stability [16].

Organometallic compounds such as metal coordination polymers and molecular complexes based on Fe, Ni, Co, Mn, Cu, or other metals have also garnered considerable attention due to their reversible electrochemical behaviour, light atom weight, availability, environmental friendliness, non-toxicity, low cost, and their ability to form various thin films and electrode composites [17]. Iron and various iron-based compounds have also been used in electrode-active materials due to their multiple reversible redox reactions and high specific capacity [18]. Ferrocene-based coordination polymers have relatively high thermal stability, two stable redox states, fast electron transfer, and excellent charge-discharge efficiency [19]. By employing modified multi-walled carbon nanotubes (MWCNTs) functionalized with ferrocene, a specific capacity of 50.0 F g^{-1} at 0.25 A g^{-1} was achieved with high cycle stability [20]. Furthermore, reduced graphene oxide (rGO) functionalized with 1,1'-bis(4-isobutyl) ferrocene displayed better electrical conductivity than rGO and demonstrated good charge-discharge performance with stable cycling [21].

In the development of TFEs or composite electroactive materials for fast charge-discharge supercapacitors, the most common method is the chemical functionalization of redox materials such as ferrocene derivatives on porous conductive electrodes. However, this synthesis process is often expensive, and the surface coverage of the bonded material is relatively low [19-21]. In surface

adsorption methods, solid active materials such as crystalline ferrocene derivatives are usually used, leading to a decrease in electrochemical efficiency. The use of liquid redox materials compared to solids can provide a more desirable interaction with carbonaceous electrodes and crystalline particles [22-24].

In this research, an attempt has been made to compare and analyse the electrochemical behaviour and energy storage capacity of two redox materials, solid ferrocene and liquid 2,2'-bis(ethyl-ferrocenyl) propane (catocene), self-assembled on the basal plane pyrolytic graphite (BPPG) electrodes. Catocene is a dark brownish-orange liquid with the chemical formula $C_{27}H_{32}Fe_2$ and an atomic mass of 282.2 g mol^{-1}, which is used as an effective catalyst in solid propellants containing ammonium perchlorate [25].

Experimental

Chemicals and apparatus

All chemical materials, such as ferrocene, sodium sulphate (Na_2SO_4), and the solvent N,N-dimethyl-formamide (DMF) with analytical grade purity, were purchased from Merck. A BPPG sheet with high electrical conductivity containing 98.69 wt.% graphite powder and 1.31 wt.% polymer with a thickness of 0.5 mm was obtained from Redoxkala Co. (Iran). Catocene liquid with 97.5 % purity containing 23.3 -to 24.4 wt.% iron was purchased from Tanyun Aerospace Materials (Yingkou) Technology Co. (China).

Electrochemical measurements, cyclic voltammetry (CV), galvanostatic charge-discharge (GCD), and electrochemical impedance spectroscopy (EIS) were performed by EG&G potentiostat-galvanostat instrument (PARSTAT 2273, Princeton Applied Research, USA), in a 1.0 M sodium sulphate solution using a three-electrode system consisting an Ag/AgCl (saturated KCl) reference electrode, a platinum auxiliary electrode with a 2.0 cm^2 surface area, and a BPPG working electrode with a geometric area of 0.2 cm^2 immersed in the electrolyte and coated with the catocene or ferrocene film. For the evaluation of the coated films on the electrode and the detection of active electrode materials, Fourier-transform infrared spectroscopy (FT-IR), attenuated total reflectance (ATR), scanning electron microscopy (SEM), energy-dispersive X-ray spectroscopy (EDS) and laser-induced breakdown spectroscopy (LIBS) elemental analysis were employed. FT-IR/ATR measurements were performed using an Infralum-FT08 spectrometer (Lumex, Russia) equipped with a DTGS detector and MIRacle™ Single Reflection ATR accessory with a diamond/ZnSe crystal plate. LIBS spectra were recorded using the LIBSCAN100 system (Photonic Applied Ltd.), which includes an Nd:YAG laser with a wavelength of 1064.0 nm, output energy of 100.0 mJ, pulse width of 2±7 ns, and a repetition rate of 1.0 to 20.0 Hz. The emitted LIBS plasma radiations were collected and transferred to the system detector capable of recording spectra in the range of 182.0 to 1057.0 nm with an accuracy of 0.04 nm. EIS studies were conducted over a frequency range of 100.0 kHz to 10.0 mHz at a DC potential of 0.5 V with a sinusoidal potential amplitude of 10.0 mV and 10 points per frequency decade.

Preparation of thin film electrodes

Working electrodes with a coating of a thin layer of catocene on BPPG electrode (Cat/BBPG) or ferrocene thin film on BPPG (Fc/BPPG) were prepared by first cleaning the graphite electrode with acetone and keeping it in a vacuum at 45.0 °C for one hour to remove surface impurities. The electrodes were then cooled to room temperature and weighed. Subsequently, 2.0 molar concentrations of redox reactants, catocene or ferrocene, were prepared in the DMF solvent. The graphite sheet

with a geometric area of 0.2 cm^2 was then immersed in the solution for 5.0 minutes. Afterwards, the solvent-soaked electrode was dried and cooled for 10.0 minutes to stabilize the catocene or ferrocene films on the surface of the graphite electrode. The weight of the electrode materials was calculated by measuring the weight difference between the initial graphite electrode and the coated electrode using a 5-digit analytical balance (Balance XPR105DR, Model). The average weight of self-assembled catocene and ferrocene on the graphite electrode was near 16.0 and 11.0 mg cm^{-2}, respectively.

Electrochemical tests

Cyclic voltammetry measurements were conducted in a three-electrode cell in 0.1 M Na_2SO_4 electrolyte solution at potential scan rates ranging from 20 to 140 mV s^{-1} and at the ambient temperature of 28-30 °C. The specific capacitance of the working electrode can be obtained from the voltammetry surface area according to equation (1) [1,28]:

$$C_{sp} = \frac{1}{2mv\Delta V}\int i(V)\mathrm{d}V \quad (1)$$

In equation (1), C_{sp} / F $g^{-1}$is the specific capacitance, m / g is the mass of self-assembled catocene or ferrocene on the working electrode, ν / V s^{-1} is the potential scan rate, $\int i(V)\mathrm{d}V$ is the area under the cyclic voltammetry curve in ampere-volts, and ΔV / V is the potential window.

Galvanostatic charge-discharge tests were conducted at current densities ranging from 1.0 to 10.0 A g^{-1}, and the specific capacitance was calculated according to equation (2) [1]:

$$C_{sp} = \frac{I\Delta t}{m\Delta V} \quad (2)$$

where I / A is the discharge current and Δt / s is the discharge time. Additionally, the specific energy density (E / Wh kg^{-1}) can be calculated using equation (3)[27]:

$$E = \frac{1}{2\times 3.6}C_{sp}\left(\Delta V\right)^2 \quad (3)$$

Here, ΔV is the operational potential window, and C_{sp} is the specific capacitance of the fabricated electrode. Also, the specific power density P / kW kg^{-1} is described in equation (4) [29]:

$$P = \frac{3.6E}{\Delta t} \quad (4)$$

where E / Wh kg^{-1} and t / s are specific energy density and discharge time, respectively.

Furthermore, an asymmetric supercapacitor was assembled using a graphite electrode as the negative electrode, Cat/BPPG or Fc/BPPG as the positive electrode, and a cellulose filter paper as the dielectric. Before electrochemical tests, the electrodes and dielectric were soaked in 0.1 M Na_2SO_4 electrolyte, and all experiments were conducted under laboratory temperature conditions. For potentiostaic or galvanostatic tests in the two-electrode configurations, the reference and auxiliary electrodes were connected, and GCD tests were recorded in the voltage window of 0.0 to 1.7 V.

Results and discussion

Characterization of electrode materials

Various surface techniques, including SEM, EDS, LIBS, and FT-IR/ATR, were utilized to assess the quality and quantity of catocene and ferrocene films formed on the relatively smooth surface of BPPG electrodes. SEM images and the distribution of Fe element with EDS mapping on the surfaces of Cat/BPPG and Fc/BPPG electrodes are depicted in Figure 1. It can be observed that iron atoms

from catocene and ferrocene are distributed with relatively low concentrations and almost uniform distribution across the entire mapped window. Upon closer evaluation of SEM images, crystalline solid particles of ferrocene with partial iron enrichment are also observed. The self-assembled liquid catocene on graphite is expected to exhibit a more uniform distribution than solid ferrocene. A homogeneous and thin layer distribution can accelerate the kinetics of electrochemical reactions, leading to increased efficiency in redox reactions.

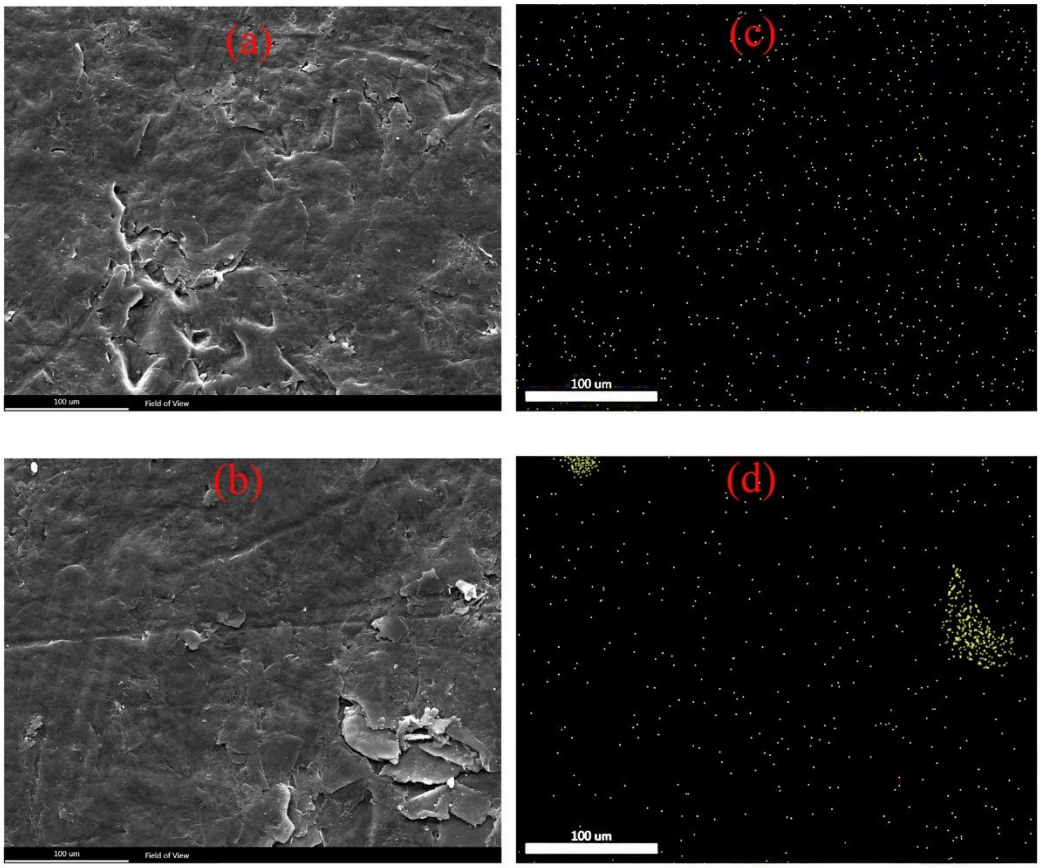

Figure 1. *SEM images of Cat/BPPG (a) and Fc/BPPG (b) and EDS mappings for Fe atoms of catocene (c) and ferrocene (d) thin films on the BPPG electrode*

Elemental analysis using EDS and LIBS of the two prepared electrodes is presented in Figure 2. EDS analysis provides a more accurate assessment of the elemental content and metal components of the films on surfaces due to the lower penetration ability of electrons into solid surfaces compared to X-ray photons. Impurities of some elements such as Ca, Mn, Fe, Ni, Zn, or others have been reported in graphite powders and their composites, depending on the production process [28]. According to Figure 2, EDS on the Cat/BPPG and Fc/BPPG surface indicates a nearly 6.0±2.0 atomic percent of iron on the electrode surfaces with dimensions of 500×500 µm. Furthermore, the surface analysis of electrodes using the highly sensitive LIBS technique equipped with an Nd: YAG laser with a wavelength of 1064 nm, output energy of 100.0 mJ, and pulse width of 2±7 nanoseconds was conducted in air. For the iron element, around 27 emission lines were reported, including 20 atomic emission lines (Fe I) and 7 ionic emission lines (Fe II), with the strongest emission line observed at 374.55 nm for Fe I [29]. Analysis of atomic spectra with the NIST LIBS database and NIST atomic spectra database on the LIBS spectra of various samples in Figure 2 shows that the presence of Fe element in BPPG surface is negligible. However, in the two electrodes modified with ferrocene and catocene, the presence of iron is noticeable in the wavelengths of 374 nm and the range of 230 to 275 nm. Atomic iron has various emission lines at wavelengths 249, 252, 272, 302, 357, 374, and

383 nm, and iron ion emission lines at 238, 259 and 274 nm. At about 390 nm, broad emission peaks due to carbon atoms or CN bonds resulting from the reaction with carbon and nitrogen in the air are observed. Atomic emission ranges of various carbon types at 248, 251, 284, 392, 426, 659 and 722 nm have been reported. Additionally, emission peaks at 600, 575, 567, 520 and 500 nm correspond to nitrogen [30].

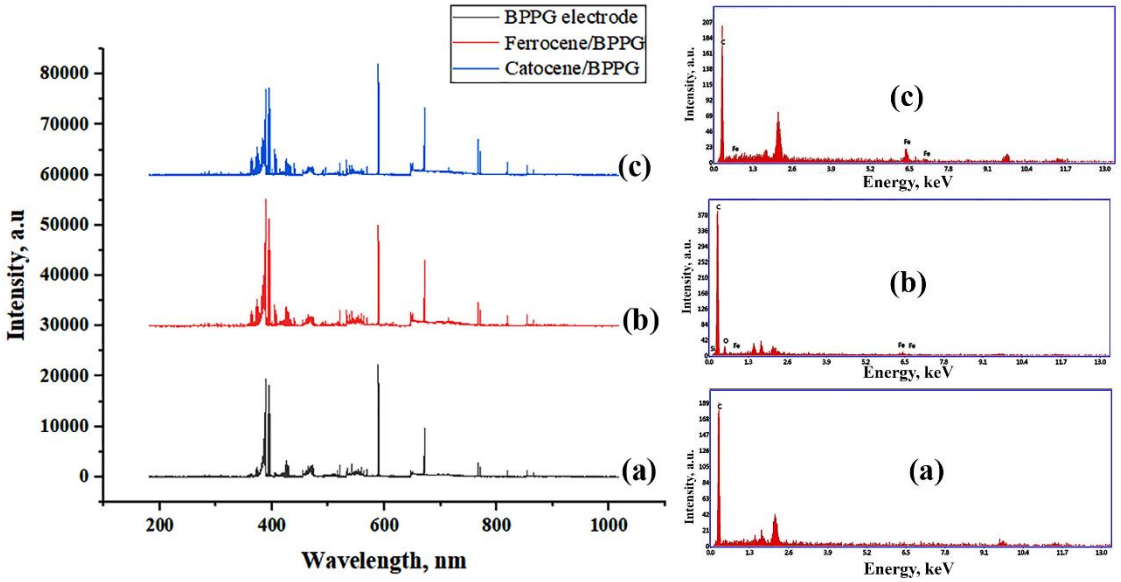

Figure 2. *Elemental analysis by energy dispersive x-ray spectroscopy (EDS) (right) and laser-induced breakdown spectroscopy (LIBS) (left) of: a) BPPG, b) BPPG coated with ferrocene thin film, and c) BPPG coated with catocene thin film*

Fourier transform infrared spectroscopy (FT-IR) is also suitable for detecting molecular functional groups and films created on electrodes. By examining the attenuated total reflectance (ATR) spectra of Fc/BPPG and Cat/BPPG electrodes (see Figure 3), the presence of components was not well-detected due to the low concentration of ferrocene or catocene films on the electrode surfaces, and some weak peaks were observed near 3000 cm^{-1} wave number. Figure 3 presents FT-IR spectra of pure ferrocene and catocene, as well as ATR spectra of the modified electrodes.

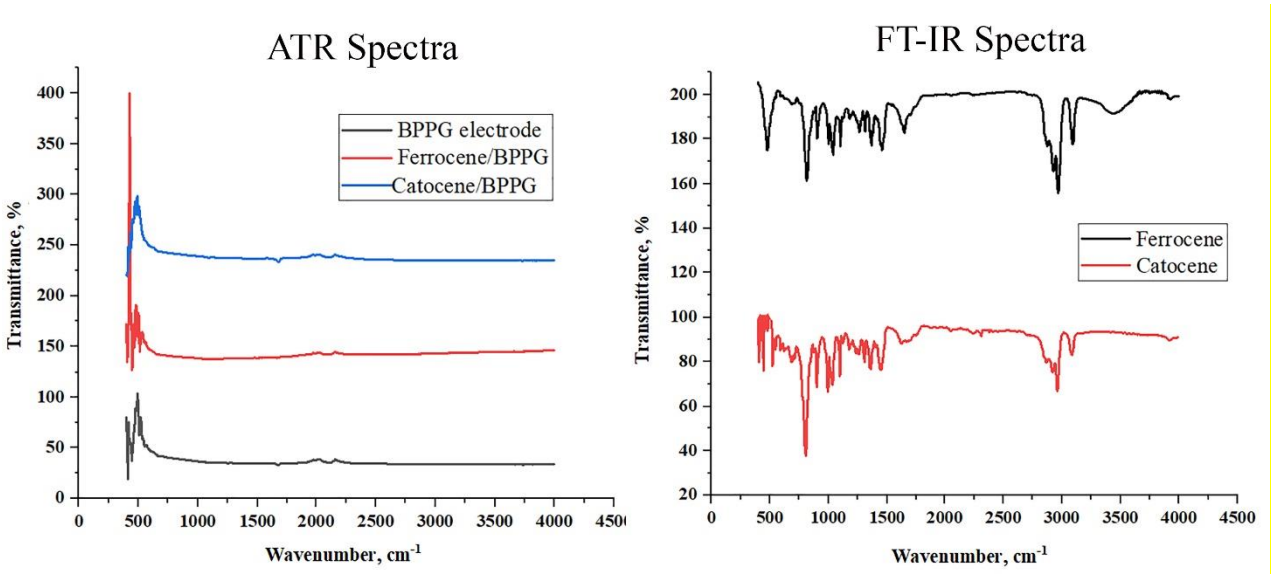

Figure 3. *FT-IR spectra of pure catocene and ferrocene (right) and ATR spectra of modified BPPG electrodes (left)*

For ferrocene, the features observed are consistent with the vibrational characteristics of cyclopentadienyl moieties, including C-H stretching (2840 to 3100 cm^{-1}), aromatic C-H asymmetric stretching vibrations (1566 to 1750 cm^{-1}), C=C phenyl stretching vibrations (1375 / 1465 cm^{-1}), C-H bending of methylene groups (985 to 995 / 905 to 915 cm^{-1}), C=C bending (815 cm^{-1}), and C-H bending vibrations (1030 cm^{-1}) [31]. Similar peaks are also observed for catocene FT-IR spectrum.

Voltammetry studies

Cyclic voltammetry was performed on liquid catocene-coated graphite electrode (Cat/BPPG), ferrocene-coated graphite electrode (Fc/BPPG), and bare graphite electrode (BPPG) in a three-electrode system with 1.0 M Na_2SO_4 electrolyte solution. The investigation covered the potential range of -0.5 to 2.0 V *vs*. Ag/AgCl at different scan rates from 20.0 to 140 mV s^{-1}. Figure 4 illustrates typical CV curves of the samples at various scan rates, showing two main peaks associated with the oxidation-reduction processes on Fc/BPPG and Cat/BPPG electrodes.

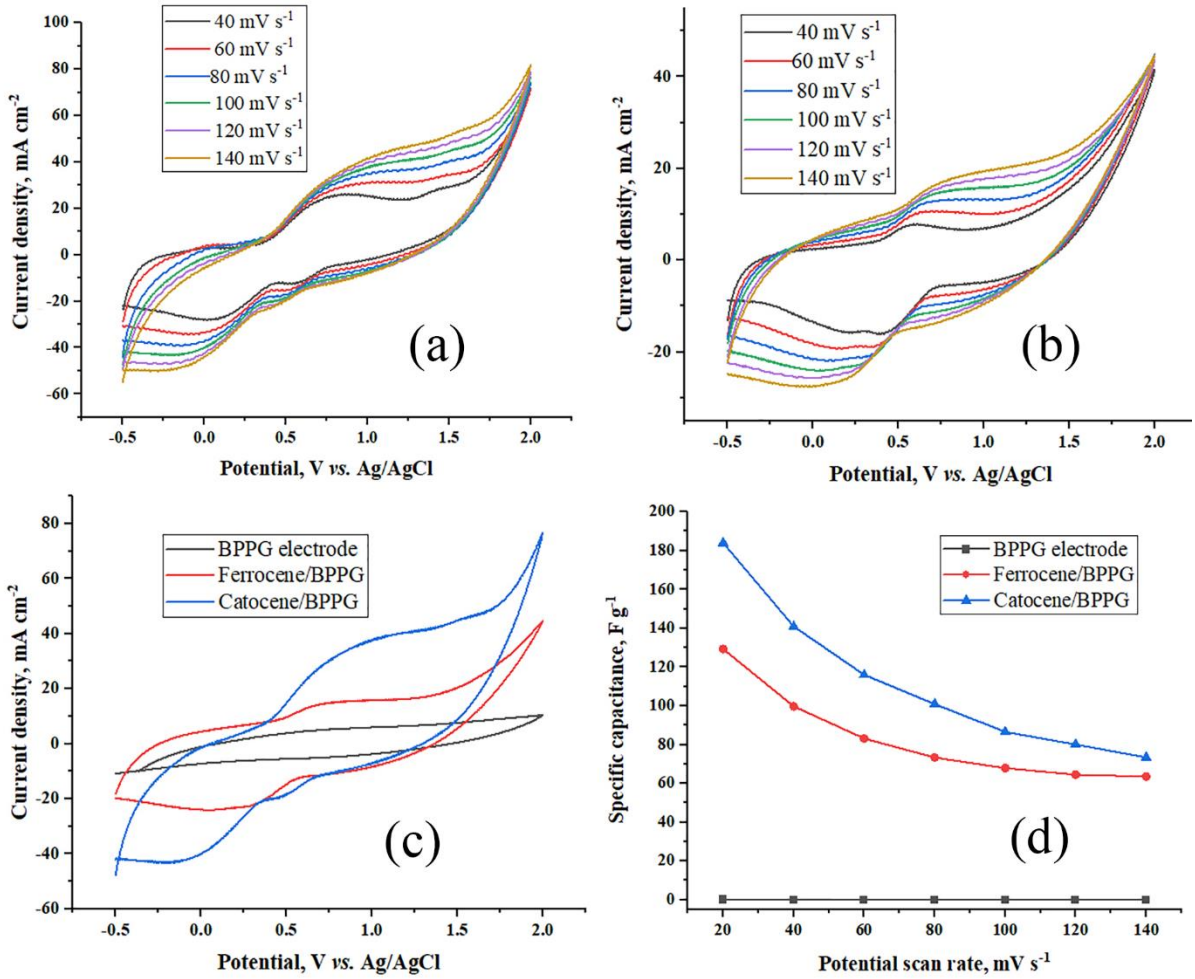

Figure 4. *Supercapacitive performance of modified BPPG electrodes assessed from three-electrode measurements in 1.0 M Na_2SO_4. CV curves of (a) catocene thin film BPPG electrode and (b) ferrocene thin film BPPG electrode at different scan rates, and (c) comparison of CV curves at 100.0 mV s^{-1}. (d) Specific capacitance derived from (a) and (b)*

Similar to the redox processes of ferrocene derivatives [23-32], ferrocene is usually oxidized to $Fe(C_2H_5)_2^+$ with an initial oxidation potential around 0.4 V. The Fe oxidation state in ferrocene or catocene is +2, and the cyclopentadienyl (C_5H_5) ligands carry a -1 charge. The reverse potential scan also exhibits a quasi-reversible reduction of $Fe(C_2H_5)_2^+$. Similar behaviour is observed for catocene. This substance is commonly used in defence and aerospace industries. It contains a small amount

of four isomeric compounds with different substitution positions for ethyl groups and di-ferrocenyl propane compounds, making their separation challenging due to nearly identical physical and chemical properties [33]. The presence of these impurities in catocene leads to an increase in the oxidation-reduction potential range of this iron complex and the appearance of a weak oxidation peak after 1.0 V and its corresponding reduction at +0.5 V. Of course, the generation of consecutive peaks in capacitors can improve their charge-discharge behaviour. With an increase in the potential scan rate, the oxidation peaks shift towards more positive potentials, and reduction peaks shift towards more negative potentials. This is because working electrodes have a low internal resistance, and a shorter time is available for the redox reactions. Additionally, with increasing scan rates, the area under CV curves and their currents increases. The anodic peak currents of catocene and ferrocene increased linearly with the square root of the scan rate. The following equations were obtained, respectively: $I = 118.49\,\nu^{1/2} + 2.07$, $R^2 = 0.9942$, and $I = 61.67\ \nu^{1/2} - 4.62$, $R^2 = 0.9985$, suggesting that the electrochemical reactions of modified electrodes are diffusion-controlled processes with quasi-reversible behaviour [34], and the related supercapacitor can be classified as a battery-like capacitor [28,36].

Trasatti's analysis method was utilized to further evaluate the contribution of EDLC and the quasi-reversible redox process with diffusion-controlled behaviour [37,46-47]. As mentioned in the literature [27], EDLC occurs on the outer surface of the electrode and contributes to the outer capacitance (C_{out}), which is assumed to be constant across the range of potential scanning rates. The redox contribution of capacitance is inner capacitance (C_{in}), controlled by semi-infinite linear diffusion with a rate proportional to $\nu^{-1/2}$. Also, the entire capacitive behaviour (C_{total}) is assumed to be divided into the contribution of the outer surface and inner surfaces of the electrode, as shown in equation 5 [27]:

$$C_{total} = C_{out} + C_{in} \quad (5)$$

Table 1 shows the capacitance contribution ratio analyzed based on the Trasatti method and the calculated areal capacitances at various potential scan rates obtained from Figure 4. It can be clearly seen that the charge storage in the Cat/BPPG and Fc/BPPG electrodes originates mainly from the battery-like contributions (93.75 and 78.02 %, respectively).

Table 1. *Capacitance contribution of the electrodes as analyzed by the Trasatti method and the areal capacitance (F cm^{-2}) based on CV curves shown in Fig. 4 (a-b)*

Potential scan rate, mV s^{-1}		Areal capacitance, F cm^{-2}		
		BPPG electrode	Cat/BPPG	Fc/BPPG
20.0		0.08	2.94	1.42
40.0		0.06	2.25	1.1
60.0		0.05	1.86	0.91
80.0		0.044	1.61	0.81
100.0		0.035	1.38	0.75
C_{total} / F cm^{-2}		0.16	44.64	5.60
C_{out} / F cm^{-2}		0.14	2.79	1.23
C_{in} / F cm^{-2}		0.020	41.85	4.37
Capacitance contribution, %	Battery like	12.70	93.75	78.02
	EDLC	87.30	6.25	21.98

In the rate-determining step of the oxidation reactions, the value of αn_α (where α is the charge transfer coefficient and n_α is the number of electrons involved in the rate-determining step) was calculated at a typical scan rate potential of 40.0 mV s^{-1}, according to the equation $\alpha n_\alpha = 0.048/(E_p - E_{p/2})$.

In this equation, E_p is the potential of the anodic peak, and $E_{p/2}$ is the potential at half the anodic peak current. Calculations indicated that the value of αn_α for the oxidation of catocene and ferrocene on the BPPG electrode were 0.16 and 0.48, respectively. The higher value of α for ferrocene indicates a lower energy barrier path for forming the activated complex, overcoming the activation energy of electrochemical reactions. On the other hand, according to the voltammetry curves in Figure 4c, it is observed that the anodic current density for catocene oxidation is almost doubled compared to ferrocene. Figure 4d also shows that the specific capacitance of the electrode with a catocene film is higher than that with a ferrocene film. Here, the surface concentration of electroactive materials or surface coverage (Γ) was calculated according to equation (6) [38]:

$$\Gamma = \frac{Q}{nFA} \quad (6)$$

In this equation, Q is the area under the oxidation peak in the CV of the modified electrodes, n is the number of electrons participating in the reaction (n = 1 in the present case), A is the electrode surface area, and F is the Faraday constant. The surface coverage (Γ) for the electrodes modified with catocene or ferrocene at different potential scan rates is presented in Table 2. It is observed that as the scan rate increases, the value Γ decreases. Furthermore, the molar coverage of catocene on graphite is approximately 50 to 75 % higher than that of ferrocene.

The electrode substrate and porosity are the same for both Cat/BPPG and Fc/BPPG electrodes. However, the faradaic reaction efficiency and capacity of liquid catocene, despite having a higher molar mass (282.2 g mol^{-1}) compared to ferrocene (186.04 g mol^{-1}), have increased. The main factors contributing to the enhanced performance of the liquid redox material catocene are more uniform distribution and more effective interaction of the liquid catocene thin film than solid ferrocene film on the graphite BPPG electrode.

Table 2. *Effect of potential scan rate on the surface coverage of catocene and ferrocene thin films on BPPG in 1.0 M Na_2SO_4*

v / mV s^{-1}	Q / mC		Γ / μmol cm^{-2}	
	Catocene	Ferrocene	Catocene	Ferrocene
40.0	677.22	389.14	7.02	4.03
60.0	560.28	326.84	5.81	3.39
80.0	469.76	286.32	4.87	2.97
100.0	400.95	254.03	4.16	2.63
120.0	351.86	225.62	3.65	2.34
140.0	310.48	208.05	3.22	2.16

Electrochemical impedance spectroscopy and galvanostatic charge-discharge studies

Electrochemical impedance spectroscopy studies at a potential of +0.5 V, as depicted in the Nyquist diagram in Figure 5a, show a slightly depressed capacitive semicircles at high frequencies related to the charge-transfer resistance and double-layer capacitance. Table 3 lists the values of impedance parameters calculated by fitting the electrical equivalent circuit (EEC) in Figure 5a to the experimental results. The goodness of the fit can be judged by the estimated relative errors presented in the parentheses. According to the values of the electrical equivalent elements reported in this table, the charge transfer resistance (R_{ct}) for ferrocene and catocene is 235.1 (±2.7 %) Ω cm² and 164.9 (±2.7 %) Ω cm², respectively. The apparent electron transfer rate constant (K_{app}) has an inverse relationship with R_{ct} on Nyquist diagrams. In other words, with a decrease in R_{ct}, the electrode reaction rates increase [34]. Therefore, the reaction rate at a constant potential for

catocene is nearly 40 % higher than that for ferrocene. In EIS studies, an appropriate equivalent circuit for the recorded Nyquist semicircles for modified electrodes is plotted in the inset of Figure 5a. The modelled equivalent circuits contain the solution resistance (R_s), the charge-transfer resistance of the oxidation step (R_{ct}), and a constant phase element corresponding to the double-layer capacitance (CPE_{dl}). The impedance of CPE_{dl} (Z_{CPE}) and infinite Warburg (Z_w) elements can be expressed as in equations (7) and (8) [38-40]:

$$Z_{CPE} = Y_0^{-1} j^{-n} \quad (7)$$

$$Z_w = \sigma^{-1/2}(1-j) \quad (8)$$

In equation (7), Y_0 (the CPE parameter, S cm^{-2} s^n) and n (dimensionless CPE exponent reflecting the roughness of the electrode surface) are two parameters independent of frequency, σ the Warburg impedance coefficient ($\Omega\, s^{-1/2}\, cm^2$) associated with the diffusivity in the electronic system; $j = -1^{1/2}$ and $\omega = 2\pi f$ is the angular frequency.

Figure 5 also presents the galvanostatic charge/discharge curves of the samples at different current densities within the potential window -0.5 to +1.2 V. It is observed that the discharge time of the samples increases with a decrease in current density.

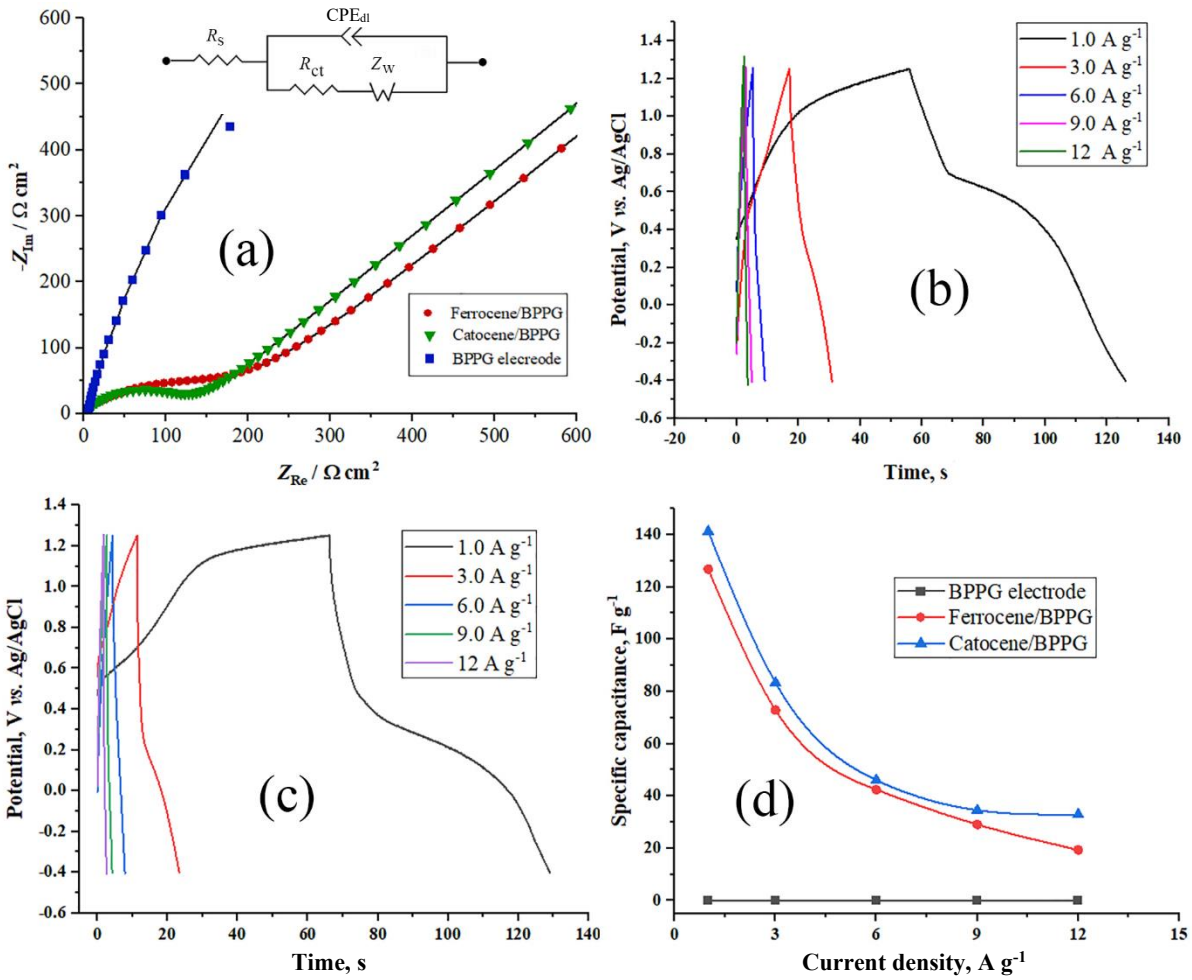

Figure 5. *a) Nyquist diagram and equivalent circuit of modified electrodes for EIS studies by applying a bias of +0.5 V and an AC voltage of 10.0 mV amplitude in a frequency range from 100.0 kHz to 10 Hz in 1.0 M Na_2SO_4; b) GCD curves of Cat/BPPG, and c) Fc/BPPG at various current densities; d) specific capacitance versus current density for electrodes with the geometric area of 0.2 cm^2*

The specific capacitance (F g^{-1}) of the electrodes is calculated from their discharge curves at different current densities, and the results are presented in Figure 5d. By comparing GCD curves of

Cat/BPPG and Fc/BPPG samples at different current densities, the specific capacitance and performance of catocene-based film electrodes are 10-15 F g^{-1} higher. The specific capacitance decreases with an increase in current density, likely due to mass transfer limitations and the diffusive mechanism of redox materials. The solid nature of ferrocene compared to the liquid catocene may lead to the formation of crystalline particles and aggregation of iron complex concentrations on the BPPG electrode surface, leading to reduced availability and performance of solid particles. SEM images of the Fc/BPPG electrode presented in Figure 1 also qualify the presence of some crystalline particles and localized iron concentrations on EDS mappings. Additionally, it appears that the van der Waals interaction of catocene molecules with the graphite surface is higher than that of ferrocene due to the more hydrophobic nature of ethyldicyclopentadienyl ligands compared to cyclopenta-1,3-diene.

Table 3. *The values of electrode impedance parameters and the corresponding percentage relative errors for the oxidation of self-assembled catocene and ferrocene thin films on BPPG in 1.0 M Na_2SO_4*

Electrode	R_s / Ω cm^2	R_{ct}/ Ω cm^2	CPE		σ / Ω $s^{-1/2}$ cm^2
			Y_0 / μS cm^{-2} s^n	n	
BPPG electrode	6.48	4645.6 (4.3 %)	0.01340 (3.2 %)	0.5500 (2.8 %)	--
Fc/BPPG	7.10	235.1 (3.0 %)	0.06447 (1.9 %)	0.5480 (3.3 %)	1753.1 (2.6 %)
Cat/BPPG	6.90	164.9 (4.4 %)	0.08553 (3.1 %)	0.7041 (2.7 %)	1156.9 (0.25 %)

Due to the favourable performance of the liquid redox material catocene at a positive potential, it was decided to construct an asymmetrical supercapacitor by pairing it with a graphite negative electrode saturated with electrolyte, as described in the experimental section, and evaluate its performance. The aim was solely to compare the behaviour of the new redox material catocene with ferrocene. According to studies mentioned in the previous section, at a potential scan rate of 20.0 mV s^{-1}, a specific capacitance close to 185 F g^{-1} for catocene and 125.0 F g^{-1} for ferrocene thin film electrodes can be achieved.

Galvanostatic charge/discharge tests were performed on a two-electrode setup in the voltage window of 0.0-1.7 V. The energy and power densities of the samples were calculated according to equations (3) and (4). Ragone plots (energy density versus power density) of the supercapacitors are presented in Figure 6.

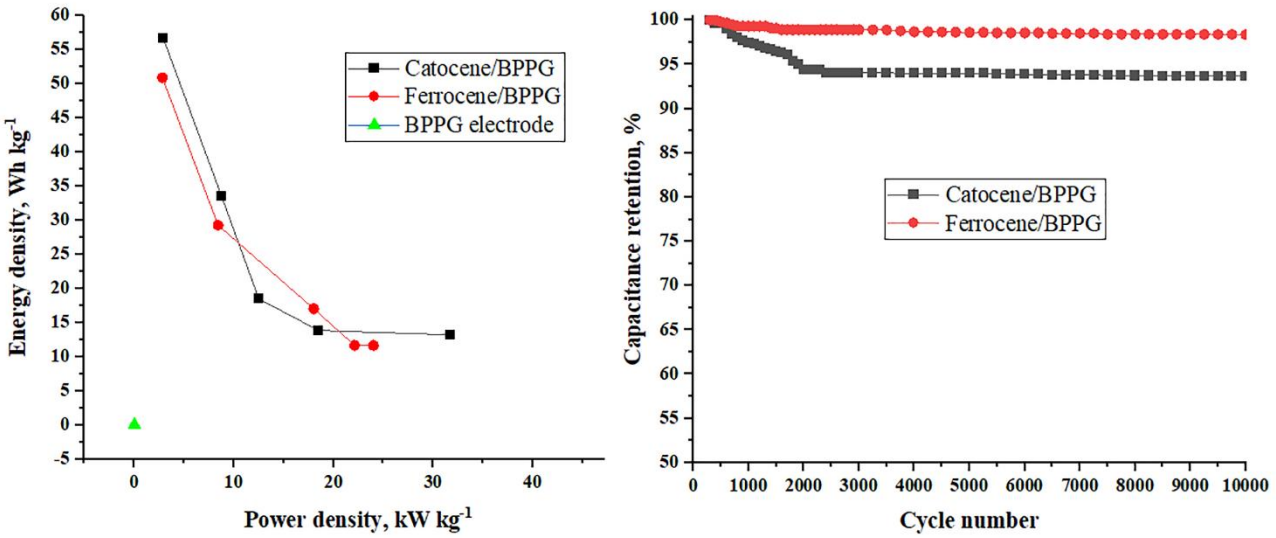

Figure 6. *(a) Ragone plots of Cat/BPPG and Fc/BPPG asymmetrical supercapacitor; (b) cycling stability of two asymmetrical supercapacitors at a current density of 5.0 A g^{-1} and 1.0 M Na_2SO_4 electrolyte*

Additionally, cyclic stability tests were conducted at a current density of 5.0 A g^{-1} for 10000 GCD cycles. The constructed capacitor with catocene exhibited an energy density of 56.7 Wh kg^{-1} at a power density of 2.9 kW kg^{-1}, while the capacitor based on ferrocene showed an energy density of 50.9 Wh kg^{-1} at a power density of 2.8 kW kg^{-1}. Moreover, with an increase in power density, the energy density values exhibit a decreasing trend. The overall capacitance of the capacitors in consecutive charge-discharge cycles shows a slight reduction over 10000 cycles. After these GCD cycles, the electrode capacity of Cat/BPPG decreases by approximately 6.3 %, and Fc/BPPG decreases by nearly 3 %. The irreversible oxidation products often cause electrode surface fouling, reducing the effectiveness of redox reactions at working electrodes [41]. The lower performance of Cat/BPPG in GCD cycles tests can be caused by the partial destruction of the catocene molecule compared to ferrocene at high oxidation potentials and its conversion to Fe_2O_3 with a more irreversible electrochemical behaviour [42-43].

Here, the supercapacitance efficiency of some similar electrodes is compared in Table 4. It is observed that the self-assembled catocene on the BPPG electrode has a relatively high power density and discharge kinetics with suitable specific capacity. Of course, the main goal of this research is to compare the electrochemical efficiency of liquid catocene with solid ferrocene on the flat surface of BPPG. Certainly, by using more efficient carbon electrodes such as rGO or MWCNTs, the performance of these materials can be expected to be increased. By utilizing multi-walled carbon nanotubes (MWCNTs) functionalized with ferrocene, a specific capacitance of 50.0 F g^{-1} at discharge current density of 0.25 A g^{-1} has been recorded [20]. Cat/BPPG shows the specific capacitance of 141.2 and 57.0 F g^{-1} at current densities of 1.0 and 5.0 A g^{-1}, respectively. Considering the high production stages and expensive cost of functionalized electrode materials and the limited amount of redox materials adhering under these conditions, it seems that the use of liquid catocene could also be a suitable approach for enhancing the performance of electrochemical capacitors.

Table 4. *Supercapacitor performances of some carbon-modified electrodes taken from the literature*

Electrode material	Electrolyte	Current density, A g^{-1}	Specific capacity, F g^{-1}	Energy density, Wh kg^{-1}	Power density, kW kg^{-1}	Cycles	Stability, %	Ref.
MnS/GO/PANI/GE[a]	3 M KOH	3.8 1.0	484 773	-	-	-	-	[44]
Ag-Ag_2O/PPy/GE[b]	0.1 M H_2SO_4	2.0	500	23.6	0.51	5000	62	[45]
ssDNA/rGO[c]	1 M KOH		129	-	-	10000	92	[46]
MnO_2/CF[d]	2.0 M Li_2SO_4	0.2	187.5	-	-	10000	99.0	[47]
$NiFe_2O_4$/CF[e]	3.0 M KOH	1.0	490	39	0.41	5000	94.2	[48]
Fc-MWCNTs[f]	2.0 M KOH	0.25	50	-	-	5000	90.8	[20]
Cat/BPPG	1.0 M Na_2SO_4	1.0 5.0	141.2 57.0	56.7 25.5	2.9 11.8	10000	93.7	This work

[a]Manganese sulfide (MnS)/graphene oxide (GO)/ polyaniline (PANI) nanocomposites on graphite electrode
[b]Ag-Ag_2O/polypyrrole (PPy) nano composite on graphite electrode
[c]Single-stranded deoxyribonucleic acid (ssDNA) functionalized reduced graphene oxide
[d]Binder-free electro-deposited MnO_2 @3D carbon felt network
[e]Nickel ferrite coated on carbon felt
[f]Ferrocene functionalized multi-walled carbon nanotubes

Conclusion

In summary, this study compared the super-capacitive behaviour of two redoxes of liquid catocene, and solid ferrocene, on a basal plane pyroletic graphite electrode. Thin layers of these materials were self-assembled on the graphite electrode, and their super-capacitive behaviours were compared in an aqueous sodium sulphate electrolyte. The liquid catocene demonstrated a more uniform distribution

and better interaction with the BPPG surface than ferrocene, with its surface molar coverage up to 75 % higher. In voltammetric studies, this material exhibited a specific capacitance close to 185.0 F g^{-1} at a potential scan rate of 20.0 mV s^{-1}, compared to 125.0 F g^{-1} for ferrocene, and provided lower charge transfer resistance during oxidation. In a way, the energy density of the asymmetrical capacitor based on catocene was measured at 56.7 Wh kg^{-1} at a power density of 2.9 kW kg^{-1}, while the ferrocene-based capacitor showed an energy density of 50.9 Wh kg^{-1} at a power density of 2.8 kW kg^{-1}, and both capacitors maintained nearly 93.7 and 97.0 % of their overall capacitance in consecutive 10000 charge-discharge cycles, respectively. The calculation of capacitance contribution ratio analysed by Trasatti's method, showed that the charge storage in the Cat/BPPG and Fc/BPPG electrodes originates mainly from the battery-like contributions (93.75 and 78.02 %, respectively). Considering the high production stages and expensive cost of chemically functionalized carbonaceous electrodes with redox materials, the use of liquid redox materials such as catocene appears to be a suitable solution for improving the performance of electrochemical capacitors.

Acknowledgements: The authors are grateful for the financial support of this work by Malek-Ashtar University of Technology (I.R. Iran).

Disclosure statement: The authors declare that they have no known competing financial interests or personal relationships that could have appeared to influence the work reported in this paper.

References

[1] S. Sharma, P. Chand, Supercapacitor and electrochemical techniques, *Results in Chemistry* **5** (2023) 100885. https://doi.org/10.1016/J.RECHEM.2023.100885

[2] J. Qiu, H. Zhao, Y. Lei, Emerging smart design of electrodes for micro-supercapacitors, *SmartMat* **3** (2022) 447-473. https://doi.org/10.1002/SMM2.1094

[3] N. S. Shaikh, S. B. Ubale, V. J. Mane, J. S. Shaikh, V. C. Lokhande, S. Praserthdam, C. D. Lokhande, P. Kanjanaboos, Novel electrodes for supercapacitor: Conducting polymers, metal oxides, chalcogenides, carbides, nitrides, MXenes, and their composites with graphene, *Journal of Alloys and Compounds* **893** (2022) 161998. https://doi.org/10.1016/J.JALLCOM.2021.161998

[4] S. S. Shah, M. A. Aziz, W. Mahfoz, M. Akhtaruzzaman, *Types of Supercapacitors, in: Biomass-Based Supercapacitors Design, Fabrication and Sustainability,* John Wiley & Sons, Ltd, 2023, pp. 93-104. https://doi.org/10.1002/9781119866435.CH6

[5] S. S. Rajaputra, N. Pennada, A. Yerramilli, N. M. Kummara, Graphene based sulfonated polyvinyl alcohol hydrogel nanocomposite for flexible supercapacitors, *Journal of Electrochemical Science and Engineering* **11** (2021) 197-207. https://doi.org/10.5599/JESE.1031

[6] V. N. K. S. K. Nersu, B. R. Annepu, S. S. B. Patcha, S. S. Rajaputra, Rice husk char as a potential electrode material for supercapacitors, *Journal of Electrochemical Science and Engineering*, **12** (2022) 451-462. https://doi.org/10.5599/JESE.1310

[7] M. S. Khan, P. Shakya, N. Bhardwaj, D. Jhankal, A. K. Sharma, M. K. Banerjee, K. Sachdev, Chemical vapor deposited graphene-based quasi-solid-state ultrathin and flexible sodium-ion supercapacitor, *Journal of Electrochemical Science and Engineering* **12** (2022) 799-813. https://doi.org/10.5599/JESE.1411

[8] S. Tomar, V. K. Singh, Cobalt and copper-based metal-organic frameworks synthesis and their supercapacitor application, *Journal of Electrochemical Science and Engineering* **14** (2024) 163–175. https://doi.org/10.5599/JESE.2096

[9] R. Maheswaran, B. P. Shanmugavel, A Critical Review of the Role of Carbon Nanotubes in the Progress of Next-Generation Electronic Applications, *Journal of Electronic Materials* **51** (2022) 2786-2800. https://doi.org/10.1007/S11664-022-09516-8/FIGURES/12

[10] S. Damiri, H. Y. Varzaneh, H. R. Ebrahimi, PEG-assisted electrochemical growth of lead oxide nanodendrites with strongly enhanced charge storage capacity, *Materials Letters* **65** (2011) 2598-2600. https://doi.org/10.1016/J.MATLET.2011.06.024

[11] M. Yu, X. Feng, Thin-Film Electrode-Based Supercapacitors, *Joule* **3** (2019) 338-360. https://doi.org/10.1016/J.JOULE.2018.12.012

[12] B. Asbani, G. Buvat, J. Freixas, M. Huvé, D. Troadec, P. Roussel, T. Brousse, C. Lethien, Ultra-high areal capacitance and high rate capability RuO_2 thin film electrodes for 3D micro-supercapacitors, *Energy Storage Materials* **42** (2021) 259-267. https://doi.org/10.1016/J.ENSM.2021.07.038

[13] S. Tanwar, A. Arya, A. Gaur, A. L. Sharma, Transition metal dichalcogenide (TMDs) electrodes for supercapacitors: a comprehensive review, *Journal of Physics: Condensed Matter*, **33** (2021) 303002. https://doi.org/10.1088/1361-648X/ABFB3C

[14] S. Panda, K. Deshmukh, S. K. Khadheer Pasha, J. Theerthagiri, S. Manickam, M. Y. Choi, MXene based emerging materials for supercapacitor applications: Recent advances, challenges, and future perspectives, *Coordination Chemistry Reviews* **462** (2022) 214518. https://doi.org/10.1016/J.CCR.2022.214518

[15] J. Wu, J. Peng, Z. Yu, Y. Zhou, Y. Guo, Z. Li, Y. Lin, K. Ruan, C. Wu, Y. Xie, Acid-Assisted Exfoliation toward Metallic Sub-nanopore TaS_2 Monolayer with High Volumetric Capacitance, *Journal of the American Chemical Society* **140** (2018) 493-498. https://doi.org/10.1021/JACS.7B11915

[16] H. Li, Y. Liu, S. Lin, H. Li, Z. Wu, L. Zhu, C. Li, X. Wang, X. Zhu, Y. Sun, Laser crystallized sandwich-like MXene/Fe_3O_4/MXene thin film electrodes for flexible supercapacitors, *Journal of Power Sources* **497** (2021) 229882. https://doi.org/10.1016/J.JPOWSOUR.2021.229882

[17] B. Chen, L. Xu, Z. Xie, W. Y. Wong, Supercapacitor electrodes based on metal-organic compounds from the first transition metal series, *EcoMat* **3** (2021) e12106. https://doi.org/10.1002/EOM2.12106

[18] X. Chen, K. Chen, H. Wang, D. Xue, Composition Design Upon Iron Element Toward Supercapacitor Electrode Materials, *Materials Focus* **4** (2015) 78-80. https://doi.org/10.1166/MAT.2015.1213

[19] M. L. Hu, M. Abbasi-Azad, B. Habibi, F. Rouhani, H. Moghanni-Bavil-Olyaei, K. G. Liu, A. Morsali, Electrochemical Applications of Ferrocene-Based Coordination Polymers, *ChemPlusChem* **85** (2020) 2397-2418. https://doi.org/10.1002/CPLU.202000584

[20] G. A. M. Ali, E. Megiel, P. Cieciórski, M. R. Thalji, J. Romański, H. Algarni, K. F. Chong, Ferrocene functionalized multi-walled carbon nanotubes as supercapacitor electrodes, *Journal of Molecular Liquids* **318** (2020) 114064. https://doi.org/10.1016/J.MOLLIQ.2020.114064

[21] R. Teimuri-Mofrad, R. Hadi, H. Abbasi, Synthesis and characterization of ferrocene-functionalized reduced graphene oxide nanocomposite as a supercapacitor electrode material, *Journal of Organometallic Chemistry* **880** (2019) 355-362. https://doi.org/10.1016/J.JORGANCHEM.2018.11.033

[22] P. Saha, V. K. Yadav, V. Gurunarayanan, R. Ramapanicker, J. K. Singh, T. G. Gopakumar, Revealing the Limits of Intermolecular Interactions: Molecular Rings of Ferrocene Derivatives on Graphite Surface, *Journal of Physical Chemistry Letters* **11** (2020) 297-302. https://doi.org/10.1021/acs.jpclett.9b03357

[23] N. Kurapati, P. Pathirathna, C. J. Ziegler, S. Amemiya, Adsorption and Electron-Transfer Mechanisms of Ferrocene Carboxylates and Sulfonates at Highly Oriented Pyrolytic Graphite, *ChemElectroChem* **6** (2019) 5651-5660. https://doi.org/10.1002/CELC.201901664
[24] S. Damiri, H. R. Pouretedal, M. Mahmoudi, Sensitive Electrocatalytic Assay of Cyclotetramethylene Tetranitramine (HMX) Explosive on Carbon Nanotube/Ag Nanocomposite Electrode, *Iranian Journal of Catalysis* **12** (2022) 69-76. https://doi.org/10.30495/ijc.2022.689576
[25] M. Sa'at, M. Yarmohammadi, M. Zamani Pedram, M. Shahidzadeh, M. S. Amini-Fazl, Evaluation of the catocene/graphene oxide nanocomposite catalytic activity on ammonium perchlorate thermal decomposition, *International Journal of Chemical Kinetics* **51** (2019) 337-345. https://doi.org/10.1002/KIN.21257
[26] A. Noori, M. F. El-Kady, M. S. Rahmanifar, R. B. Kaner, M. F. Mousavi, Towards establishing standard performance metrics for batteries, supercapacitors and beyond, *Chemical Society Reviews* **48** (2019) 1272-1341. https://doi.org/10.1039/C8CS00581H
[27] K. Liu, Z. Hu, R. Xue, J. Zhang, J. Zhu, Electropolymerization of high stable poly(3,4-ethylenedioxythiophene) in ionic liquids and its potential applications in electrochemical capacitor, *Journal of Power Sources* **179** (2008) 858-862. https://doi.org/10.1016/J.JPOWSOUR.2008.01.024
[28] M. Ghosh, K. K. Swain, P. S. Remya Devi, T. A. Chavan, A. K. Singh, M. K. Tiwari, R. Verma, Determination of impurities in graphite using synchrotron radiation based X-ray fluorescence spectrometry, *Applied Radiation and Isotopes* **128** (2017) 210-215. https://doi.org/10.1016/J.APRADISO.2017.07.025
[29] N. Idris, K. Lahna, Fadhli, M. Ramli, Study on Emission Spectral Lines of Iron, Fe in Laser-Induced Breakdown Spectroscopy (LIBS) on Soil Samples, *Journal of Physics: Conference Series* **846** (2017) 012020. https://doi.org/10.1088/1742-6596/846/1/012020
[30] Y. Ralchenko, A. Kramida, Development of NIST Atomic Databases and Online Tools, *Atoms* **8** (2020) 56. https://doi.org/10.3390/ATOMS8030056
[31] J. Shimei, W. Yue, Vibrational spectra of an open ferrocene and a half-open ferrocene. *Spectrochimica Acta Part A: Molecular and Biomolecular Spectroscopy* **55** (1999) 1025-1033. https://doi.org/10.1016/S1386-1425(98)00246-7
[32] N. G. Tsierkezos, Cyclic voltammetric studies of ferrocene in nonaqueous solvents in the temperature range from 248.15 to 298.15, *Journal of Solution Chemistry* **36** (2007) 289-302. https://doi.org/10.1007/s10953-006-9119-9
[33] L. Xiaoju, S. Qi, F. Haitao, Z. Chi, M. Xiaoyan, L. Xiaoju, S. Qi, F. Haitao, Z. Chi, M. Xiaoyan, Theoretical and experimental study on synthesis of high-content catocene. *Journal of Beijing University of Aeronautics and Astronautics* **47** (2021) 2514-2520. https://doi.org/10.13700/J.BH.1001-5965.2020.0497
[34] A. J. Bard, L. R. Faulkner, *Electrochemical Methods: Fundamentals and Applications, 2nd Edition, John Wiley & Sons,* 2001.
[35] Y. Gogotsi, R. M. Penner, Energy Storage in Nanomaterials - Capacitive, Pseudocapacitive, or Battery-like? *ACS Nano* **12** (2018) 2081-2083. https://doi.org/10.1021/acsnano.8b01914
[36] M. R. Thalji, G. A. M. Ali, P. Liu, Y. L. Zhong, K. F. Chong, $W_{18}O_{49}$ nanowires-graphene nanocomposite for asymmetric supercapacitors employing $AlCl_3$ aqueous electrolyte. *Chemical Engineering Journal* **409** (2021) 128216. https://doi.org/10.1016/J.CEJ.2020.128216
[37] W. Pholauyphon, P. Charoen-amornkitt, T. Suzuki, S. Tsushima, Perspectives on accurately analyzing cyclic voltammograms for surface- and diffusion-controlled contributions, *Electrochemistry Communications* **159** (2024) 107654. https://doi.org/10.1016/J.ELECOM.2023.107654

[38] S. Damiri, H. R. Pouretedal, A. Heidari, Fabrication of a nanostructured TiO_2/carbon nanotube composite electrode for voltammetric and impedimetric determination of NTO explosive in the water and soil samples, *International Journal of Environmental Analytical Chemistry* **96** (2016) 1059-1073. https://doi.org/10.1080/03067319.2016.1232722

[39] K. M. Košiček, K. Kvastek, V. Horvat-Radošević, Different charge storage mechanisms at some carbon electrodes in redox active electrolyte revealed by electrochemical impedance spectroscopy, *Electrochimica Acta* **195** (2016) 77-84. https://doi.org/10.1016/J.ELECTACTA.2016.02.140

[40] C. P. Zimmermann, G. M. Kranz, J. P. Eckert, L. Fadani, M. Zanetti, J. M. M. de Mello, P. R. Innocente, G. L. Colpani, M. A. Fiori, C. H. Scuracchio, Ionic Polymer-Metal Composite Coated with Polyaniline Film by Electrodeposition: A Promising IPMC/PANI Junction for Applications in Robotics and Bioengineering, *Materials Research* **26** (2023) e20220609. https://doi.org/10.1590/1980-5373-MR-2022-0609

[41] J. Jang, H. U. Cho, S. Hwang, Y. Kwak, H. Kwon, M. L. Heien, K. E. Bennet, Y. Oh, H. Shin, K. H. Lee, D. P. Jang, Understanding the different effects of fouling mechanisms on working and reference electrodes in fast-scan cyclic voltammetry for neurotransmitter detection, *Analyst* **149** (2024) 3008-3016. https://doi.org/10.1039/D3AN02205F

[42] B. Z. Jiang, T. P. Wang, Oxidation of Catocene in AP/Catocene Mixture at Low Temperature, *Propellants, Explosives, Pyrotechnics* **44** (2019) 513-518. https://doi.org/10.1002/PREP.201800168

[43] S. K. Patil, M. M. Vadiyar, S. C. Bhise, S. A. Patil, D. V. Awale, U. V. Ghorpade, J. H. Kim, A. V. Ghule, S. S. Kolekar, Hydroxy functionalized ionic liquids as promising electrolytes for supercapacitor study of α-Fe_2O_3 thin films, *Journal of Materials Science: Materials in Electronics* **28** (2017) 11738-11748. https://doi.org/10.1007/S10854-017-6978-3

[44] K. Y. Yasoda, S. Kumar, M. S. Kumar, K. Ghosh, S. K. Batabyal, Fabrication of MnS/GO/PANI nanocomposites on a highly conducting graphite electrode for supercapacitor application, *Materials Today Chemistry* **19** (2021) 100394. https://doi.org/10.1016/J.MTCHEM.2020.100394

[45] E. Karaca, D. Gökcen, N. Ö. Pekmez, K. Pekmez, Galvanostatic synthesis of nanostructured Ag-Ag_2O dispersed PPy composite on graphite electrode for supercapacitor applications. *International Journal of Energy Research* **44** (2020) 158-170. https://doi.org/10.1002/ER.4881

[46] Y. Albarqouni, G. A. M. Ali, S. P. Lee, A. R. Mohd-Hairul, H. Algarni, K. F. Chong, Dual-functional single stranded deoxyribonucleic acid for graphene oxide reduction and charge storage enhancement, *Electrochimica Acta* **399** (2021) 139366. https://doi.org/10.1016/J.ELECTACTA.2021.139366

[47] V. Prabu, K. Geetha, R. Sekar, M. Ulaganathan, Binder-Free Electro-Deposited MnO_2@3D Carbon Felt Network: A Positive Electrode for 2V Aqueous Supercapacitor, *Energy Technology* **11** (2023) 2201345. https://doi.org/10.1002/ENTE.202201345

[48] S. Azizi, M. B. Askari, S. M. Rozati, M. Masoumnezhad, Nickel ferrite coated on carbon felt for asymmetric supercapacitor, *Chemical Physics Impact* **8** (2024) 100543. https://doi.org/10.1016/J.CHPHI.2024.100543